

Figure 7 Microphotograph of the fabricated LNAs. [Color figure can be viewed in the online issue, which is available at www.interscience.wiley.com.]

4. CONCLUSION

In the BiCMOS process, the trade-off in specifications of all kind of circuits can be fully utilized for possible circuit designs. In this paper, the trade-off between the NF and linearity for LNA circuit design have been tested and verified. A good choice in the first stage of the LNA design is an HBT for a better NF, and the last stage is an MOS for better linearity. Furthermore, the circuits (HBT-MOS) designed in this paper are very useful for integration with other subcircuits in 5–6-GHz receivers IC due to its power-saving characteristic and better figure of merit.

REFERENCES

1. J.D. Cressler, SiGe HBT technology: A new contender for Si-based RF and microwave circuit applications, *IEEE Trans Microwave Theory Tech* 46 (1998), 572–589.
2. R. Götzfried, F. Beisswanger, S. Gerlach, A. Schüppen, H. Dietrich, U. Seiler, K.H. Bach, and J. Albers, RFIC's for mobile communication systems using SiGe bipolar technology, *IEEE Trans Microwave Theory Tech* 46 (1998), 661–668.
3. X. Li, T. Brogan, M. Esposito, B. Meyers, and K.O., A comparison of CMOS and SiGe LNA's and mixers for wireless LAN application, *Proc IEEE 2001 Custom Integrated Circuits Conf*, 2001, pp. 531–534.
4. L.E. Larson, Silicon technology tradeoffs for radio-frequency/mixed-signal systems-on-a-chip, *IEEE Trans Electron Device* 50 (2003), 683–699.
5. H. Hjelmgren and A. Litwin, Small-signal substrate resistance effect in RF CMOS identified through device simulations, *IEEE Trans Electron Devices* 48 (2001), 397–399.
6. F. Behbahani et al., 2.4-GHz low-IF receiver for wideband WLAN in 0.6- μm CMOS architecture and front-end, *IEEE J Solid-State Circ* 35 (2000), 1908–1916.
7. H.-K. Chen and H.-J. Chen, A 5.2-GHz CASCADE-MOS 0.35- μm BICMOS Technology Ultra-Low-Power LNA Using Novel Floating Body Method, *Microwave Opt Technol Lett* 45 (2005).
8. B. Razavi, *RF Microelectronics*, Prentice-Hall, Upper Saddle River, NJ, 1998, pp. 14–20.
9. P. Wambacq and W. Sansen, *Distortion analysis of analog integrated circuits*, Kluwer Academic, Boston, 1998.
10. K.W. Kobayashi, A.K. Oki, L.T. Tran, and D.C. Streit, Ultra-low dc power GaAs HBT S- and C-band low-noise amplifiers for portable wireless applications, *IEEE Trans MTT* 43 (1995).
11. M. Soyuer, J.O. Plouchart, H. Ainspan, and J. Burghartz, A 5.8-GHz 1-V low-noise amplifier in SiGe bipolar technology, *IEEE RFIC Symp Dig* (1997), 19–22.
12. S.P. Voinigescu and M.C. Maliepaard, 5.8-GHz and 12.6-GHz Si bipolar MMICs, *IEEE ISSCC97 Dig* (1997), 372–373.
13. E.H. Westerwick, A 5-GHz band CMOS low-noise amplifier with a 2.5-dB noise figure, *Symp VLSI Tech Syst Applic Dig* (2001), 224–227.

14. K. Runge, D. Pehlke, and B. Schiffer, On-chip mated 5.2- and 5.8-GHz differential LNAs fabricated using 0.35- μm CMOS technology, *Electron Lett* 35 (1999), 1899–1900.
15. C.-Y. Cha and S.-G. Lee, A 5.2-GHz LNA in 0.35- μm CMOS utilizing inter-stage series resonance and optimizing the substrate resistance, *IEEE J Solid-State Circ* 38 (2003), 669–672.
16. R.-C. Liu, C.-R. Lee, H. Wang, and C.-K. Wang, A 5.8-GHz two-stage high-linearity low-voltage low noise amplifier in a 0.35- μm CMOS technology [WLANs], *IEEE Radio Freq Integrated Circ (RFIC) Symp Dig*, Seattle, WA, (2002), 221–224.
17. C.-C. Tang and S.-I. Liu, Low-voltage CMOS low-noise amplifier using planar-interleaved transformer, *Electron Lett* 37 (2001), 497–498.

© 2005 Wiley Periodicals, Inc.

MODELING OF LOSSY MULTIREGION SUBSTRATES IN MICROELECTRONIC CIRCUITS USING TIME-DOMAIN SURFACE INTEGRAL EQUATIONS

Chuanyi Yang and Vikram Jandhyala

Applied Computational Electromagnetics Lab
Dept. of Electrical Engineering
University of Washington
Box 352500, Seattle WA 98195

Received 30 March 2005

ABSTRACT: In this work, the electromagnetic modeling of multiregion, finite-sized lossy substrates in microelectronic circuits is carried out utilizing time-domain surface integral equations. To reduce the additional computational complexity in the implementation caused by the decaying “wake” of the Green’s function in lossy media, the resulting temporal convolution is addressed by the creation and use of an a priori exponential fitting table for discrete distances through Prony’s method. © 2005 Wiley Periodicals, Inc. *Microwave Opt Technol Lett* 47: 68–73, 2005; Published online in Wiley InterScience (www.interscience.wiley.com). DOI 10.1002/mop.21084

Key words: time domain integral equation; lossy materials; substrate coupling; Green’s functions; coupled circuit-electromagnetic simulation

1. INTRODUCTION

With the modern microelectronic industry entering a new era featuring progressively higher speed and more highly integrated mixed-signal systems on chip, accurate modeling of distributed electromagnetic behavior of sections, which may include signal traces, power planes, substrates, and so forth, is crucial during the design flow. Driven by broadband and nonlinear circuit design [1–5], time-domain coupled electromagnetic and circuit simulation has been gaining popularity. In particular, integral-equation methods [6–14] have proven to be useful since radiation conditions are built in and only surface meshing and modeling is needed. In this work, the time-domain integral equation (TDIE) method is enhanced to model realistic loss behavior in substrates, which is a crucial component for quality-factor prediction of integrated passives, as well as potentially for thermal pattern prediction.

The EM simulation environment in emerging and future 3D integrated circuits is characterized by multiple piecewise homogeneous regions. Each region is comprised of lossy materials, which may or not have a strong impact on the overall performance. In general, for higher speed and higher sensitivity systems such as RF and analog methods, the loss is a crucial factor in determining system specifications and performance. The TDIE approach has

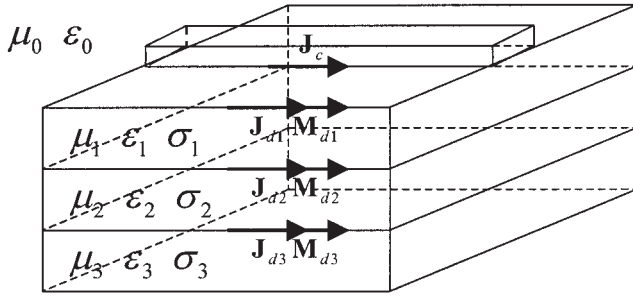


Figure 1 Multiregion substrate. The layered structure is only shown for convenience but is not required in the formulation or implementation

been shown to work with lossy material [15–18] wherein the Green’s functions, besides possessing delta functions in time, also include a broadly exponentially decaying ‘wake’. This leads to the implementation issue that the spatial integrals at retarded times have to be replaced by temporal convolutions. This convolution brings not only coding complexity, but also increases the computational cost dramatically [15, 17].

In the presented work, the multiregion substrate geometry is addressed with a TDIE solver. An equivalent-surface approach for each region is used along with the following method to tackle the lossy medium Green’s function. To circumvent the difficulty caused by the convolution in time, the decaying ‘wake’ in the Green’s function is approximated by a sum of decaying exponentials via Prony’s method. It is shown that for circuit dimensions and realistic losses, the decaying ‘wake’ changes slowly with the variation of the distance between the source and observation point. This allows the creation and use of an exponential fitting table for discrete distances. The use of the exponential models permits the convolutions in time to be computed recursively. This then achieves the purpose of reducing the computational complexity, as compared to the brute force case, to be the same as that of a TDIE solver for lossless media, except for an increased constant.

2. FORMULATION

2.1. Multiregion Substrate Modeling Using TDIE

As shown in Figure 1, the substrate may consist of multiple regions, and each region is characterized by its material property parameters μ_n , ϵ_n and σ_n . By invoking the equivalence principle, the interior material of each region is replaced by an equivalent surface S_{dk} , $k = 1, 2, \dots, n$, on which both equivalent electric current \mathbf{J}_{dk} and magnetic current \mathbf{M}_{dk} exist. On the conductor surface only an electric current \mathbf{J}_c exists.

The scattered field outside and inside each region may be written in terms of the equivalent current \mathbf{J}_{dk} , \mathbf{M}_{dk} , and \mathbf{J}_c . Here, S_{dk}^- and S_{dk}^+ indicates approaching S_{dk} from inside and outside, respectively [19]:

$$\begin{aligned} \mathbf{E}_e^{s,k}(\mathbf{J}_c, \mathbf{J}_{dk}, \mathbf{M}_{dk}) + \mathbf{E}^{inc} = 0 \quad \mathbf{r} \in S_{dk}^- \quad k = 1, 2, \dots, n \\ \mathbf{E}_d^{s,k}(\mathbf{J}_{dk}, \mathbf{M}_{dk}) = 0 \quad \mathbf{r} \in S_{dk}^+ \quad k = 1, 2, \dots, n. \end{aligned} \quad (1)$$

For the sake of formulation clarity, assume there is no conductor residing inside the substrate. By invoking a surface-impedance approximation in the time domain, the boundary condition for the electric field on the surface of the conductor is given by

$$[\mathbf{E}_c^s(\mathbf{J}_c, \mathbf{J}_{d1}, \mathbf{M}_{d1}, \dots, \mathbf{J}_{dn}, \mathbf{M}_{dn}) + \mathbf{E}^{inc}]_{\tan} = \left[Z_s^* \frac{\partial \mathbf{J}_c}{\partial t} \right]_{\tan} \quad \mathbf{r} \in S_c, \quad (2)$$

where \tan denotes the tangential part of S_c , $*$ denotes temporal convolution, and $Z_s(t)$ is the time-domain representation of surface impedance

$$Z_s(t) = \begin{cases} \sqrt{\mu/\pi\sigma t} & t > 0 \\ 0 & t < 0 \end{cases} \quad (3)$$

A detailed description on how the temporal convolution is computed efficiently can be found in [10, 23–26]. Assume the background media is lossless. For the exterior problem, currents \mathbf{J}_d , \mathbf{M}_d , and \mathbf{J}_c satisfy the following equation:

$$\begin{aligned} \mathbf{E}^{inc}(\mathbf{r}, t) = \int_s ds' \int_{-\infty}^{t-R/c_0} dt' \mu_0 G_e(R, t') * \frac{\partial \mathbf{J}(\mathbf{r}', t')}{\partial t'} \\ + \nabla \int_s ds' \int_{-\infty}^{t-R/c_0} dt' \frac{-1}{\epsilon_0} G_e(R, t') * \int_0^{t'} \nabla \cdot \mathbf{J}(\mathbf{r}', t'') dt'' + \\ \nabla \times \int_s ds' \int_{-\infty}^{t-R/c_0} dt' G_e(R, t') * \mathbf{M}(\mathbf{r}', t') \end{aligned} \quad (4)$$

$$S = S_d \cup S_c, \quad \mathbf{J} = \mathbf{J}_d \cup \mathbf{J}_c, \quad \mathbf{M} = \mathbf{M}_d,$$

and for the interior problem, currents \mathbf{J}_{dk} and \mathbf{M}_{dk} satisfy

$$\begin{aligned} 0 = \int_{s_{dk}} ds' \int_{-\infty}^{t-R/c_k} dt' \mu_k G_d(R, t') * \left(\frac{\partial \mathbf{J}_{dk}(\mathbf{r}', t')}{\partial t'} + \frac{\sigma_k}{\epsilon_k} \mathbf{J}_{dk}(\mathbf{r}', t') \right) \\ + \nabla \int_{s_{dk}} ds' \int_{-\infty}^{t-R/c_k} dt' \frac{-1}{\epsilon_k} G_d(R, t') * \int_0^{t'} \nabla \cdot \mathbf{J}_{dk}(\mathbf{r}', t'') dt'' + \\ \nabla \times \int_{s_{dk}} ds' \int_{-\infty}^{t-R/c_k} dt' G_d(R, t') * \left(\mathbf{M}_{dk}(\mathbf{r}', t') \right. \\ \left. + \frac{\sigma_k}{\epsilon_k} \int_0^{t'} \mathbf{M}_{dk}(\mathbf{r}', t'') dt'' \right) \quad k = 1, 2, \dots, n. \end{aligned} \quad (5)$$

In Eqs. (4) and (5), $R = |r - r'|$ represents the distance between source and observer; c_0 and c_k are the speed of light in the background media and inside each substrate region, respectively, and $G_e(R, t')$ is the Green’s function in the lossless background media:

$$G_e(R, t') = \frac{\delta(t - t' - R/c_0)}{4\pi R}. \quad (6)$$

However, for $G_d(R, t')$, the Green’s function in the substrate (shown below), in addition to the δ function, also includes another term due to the exponentially decaying wake, owing to the loss of the substrate [20]:

$$G_d(R, t') = \frac{\exp(-\sigma_k(t-t'))/2\varepsilon_k}{4\pi} \left[\frac{\delta(t-t'-R/c_k)}{R} + \frac{\sigma_k I_1 \left[\frac{\sigma_k}{2\varepsilon_k c_k} \sqrt{c_k^2(t-t')^2 - R^2} \right]}{2\varepsilon_k \sqrt{c_k^2(t-t')^2 - R^2}} U(t-t'-R/c_k) \right] = G_0 + G_1, \quad (7)$$

where σ_k and ε_k are the conductivity and permittivity of subregion k , respectively, I_1 is the first order modified Bessel function of the first kind, and U is the Heaviside step function. To numerically solve Eqs. (1) and (2), electric current \mathbf{J} and magnetic current \mathbf{M} are approximated in terms of spatial- and temporal-basis functions:

$$\mathbf{J}(\mathbf{r}, t) \equiv \sum_{i=1}^{N_e} \sum_{l=1}^{N_t} I_{il} T_l(t) \mathbf{f}_i(\mathbf{r}), \quad (8)$$

$$\mathbf{M}(\mathbf{r}, t) \equiv \sum_{i=1}^{N_d} \sum_{l=1}^{N_t} M_{il} T_l(t) \mathbf{g}_i(\mathbf{r}). \quad (9)$$

The spatial basis function $\mathbf{f}_i(\mathbf{r})$ used here is the well-known RWG basis function [19], and $\mathbf{g}_i(\mathbf{r}) = \mathbf{n} \times \mathbf{f}_i(\mathbf{r})$ [19], where \mathbf{n} is the unit outward normal vector. N_e and N_d are the number of edges related to electric and magnetic current, respectively. $T_l(t)$ is the temporal basis function and $T_l(t) = T(t - l\Delta t)$, where $T(t)$ is a local temporal basis function and Δt is the time step size. A variety of temporal basis functions [21, 22] have been studied in the TDIE literature for accuracy and late time stability. In this work, the simplest case of a piecewise constant is used, although the presented formulation is more general. Substituting Eqs. (9) and (10) into Eqs. (1) and (2), Galerkin testing the resulting equations in space with $\mathbf{f}_i(\mathbf{r})$, and point matching in time at time $t_l = l\Delta t$, a matrix equation is established where the electric and magnetic current weight coefficients are the unknowns:

$$\begin{bmatrix} \overline{\mathbf{Z}}_{JJ0}^{cc} & \overline{\mathbf{Z}}_{JJ0}^{cd} & \overline{\mathbf{Z}}_{JM0}^{cd} \\ \overline{\mathbf{Z}}_{JJ0}^{dc} & \overline{\mathbf{Z}}_{JJ0}^{dd} & \overline{\mathbf{Z}}_{JM0}^{dd} \\ \mathbf{0} & \overline{\mathbf{Z}}_{MJ0}^{dd} & \overline{\mathbf{Z}}_{MM0}^{dd} \end{bmatrix} \begin{bmatrix} \mathbf{J}_c(t_l) \\ \mathbf{J}_d(t_l) \\ \mathbf{M}_d(t_l) \end{bmatrix} = \sum_{k=1}^l \begin{bmatrix} \overline{\mathbf{Z}}_{JJk}^{cc} & \overline{\mathbf{Z}}_{JJk}^{cd} & \overline{\mathbf{Z}}_{JMk}^{cd} \\ \overline{\mathbf{Z}}_{JJk}^{dc} & \overline{\mathbf{Z}}_{JJk}^{dd} & \overline{\mathbf{Z}}_{JMk}^{dd} \\ \mathbf{0} & \overline{\mathbf{Z}}_{MJk}^{dd} & \overline{\mathbf{Z}}_{MMk}^{dd} \end{bmatrix} \begin{bmatrix} \mathbf{J}_c(t_{l-k}) \\ \mathbf{J}_d(t_{l-k}) \\ \mathbf{M}_d(t_{l-k}) \end{bmatrix} + \begin{bmatrix} \mathbf{SRC}_{EM}^c(t_l) \\ \mathbf{SRC}_{EM}^d(t_l) \\ \mathbf{0} \end{bmatrix}. \quad (10)$$

In the above equation, the left-hand side represents the instantaneous interaction, the first part on the right-hand side denotes the delayed interaction due to the finite speed of electromagnetic waves, and the second part is based on the incident plane-wave excitation.

2.2. Recursive Temporal Convolution

Unlike the convolution between the δ function and source, which leads to a spatial integration in retarded time, an explicit integration over time has to be done for convolution between $G_1(7)$ and the source as shown in Eq. (11), where $F(t')$ is the variation of source with time.

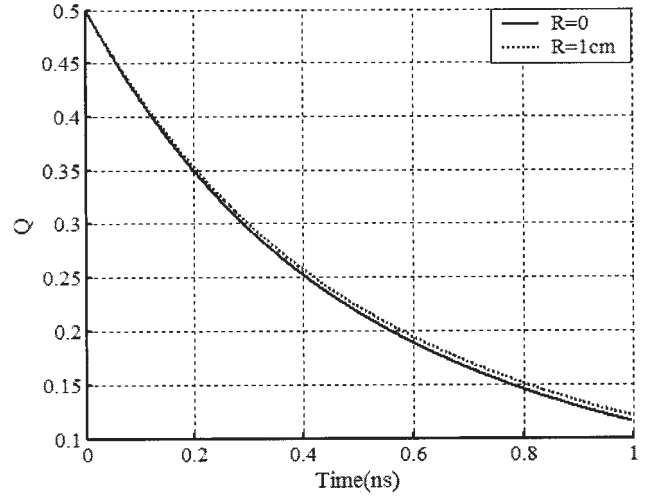


Figure 2 Plot of Q for conductivity = 0.1 s/m

$$\int_0^{t-R/c_k} G_1(t') * F(t') dt' = \int_0^{t-R/c_k} \frac{\exp(-\sigma_k(t-t'))/2\varepsilon_k}{4\pi} \frac{\sigma_k I_1 \left[\frac{\sigma_k}{2\varepsilon_k c_k} \sqrt{c_k^2(t-t')^2 - R^2} \right]}{2\varepsilon_k \sqrt{c_k^2(t-t')^2 - R^2}} U(t-t'-R/c_k) F(t') dt'. \quad (11)$$

Direct computation of the temporal convolution drastically increases the computational cost by a factor of the total number of time steps, and is therefore not practical for large simulation problems. To circumvent this difficulty, the following recursive temporal convolution scheme is used to compute the convolution efficiently. Let $t - t' = \tau + R/c_k \Rightarrow t' = t - \tau - R/c_k$. Eq. (11) has the following new forms:

$$\int_0^{t-R/c_k} \exp(-\sigma_k \tau / 2\varepsilon_k) \frac{I_1 \left[\frac{\sigma_k}{2\varepsilon_k c_k} \sqrt{c_k^2 \tau^2 + 2\tau R c_k} \right]}{\frac{\sigma_k}{2\varepsilon_k c_k} \sqrt{c_k^2 \tau^2 + 2\tau R c_k}} \times F(t - \tau - R/c_k) d\tau, \quad (12)$$

$$\text{Let } Q(\tau, R) = \exp(-\sigma_k \tau / 2\varepsilon_k) \frac{I_1 \left[\frac{\sigma_k}{2\varepsilon_k c_k} \sqrt{c_k^2 \tau^2 + 2\tau R c_k} \right]}{\frac{\sigma_k}{2\varepsilon_k c_k} \sqrt{c_k^2 \tau^2 + 2\tau R c_k}}. \quad (13)$$

Note that $Q(\tau, R)$ is a function of both τ and R . To understand how Q changes with respect to τ and R , consider $I_1(x)/x$ as follows:

$$\frac{I_1(x)}{x} = \begin{cases} B_1/x & x < 10 \\ \exp(x)/\sqrt{2\pi x^3} & x > 10. \end{cases} \quad (14)$$

As shown in Figures 2 and 3, given realistic circuit dimensions and realistic loss, $Q(\tau, R)$ changes slowly and smoothly with the variation of R , the distance between the source and the observation point. Based on this property, as indicated by Eq. (15), $Q(\tau, R)$ can be well-approximated by a summation of weighted exponentials [23–26]:

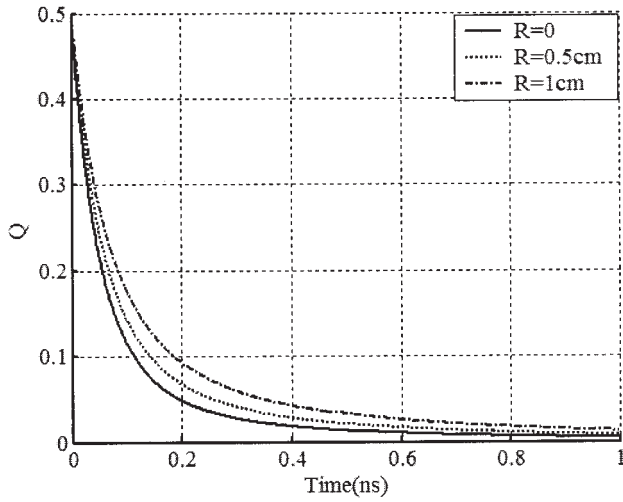


Figure 3 Plot of Q for conductivity = 1 s/m

$$Q(\tau, R) \cong \exp(-\sigma_k \tau / 2\epsilon_k) I_1 \left[\frac{\sigma_k}{2\epsilon_k c_k} \sqrt{c_k^2 \tau^2 + 2\tau R c_k} \right] - \frac{\sigma_k}{2\epsilon_k c_k} \sqrt{c_k^2 \tau^2 + 2\tau R c_k} = \sum_{i=1}^q \alpha_i \exp(\beta_i \tau / \Delta t). \quad (15)$$

It is also possible to build an exponential table for discrete distance to approximately fit $Q(\tau, R)$ from $Q(\tau, 0)$ to $Q(\tau, R_{\max})$, where R_{\max} represents the longest distance between the source and observer:

$$Q(\tau, R_k) = \sum_{i=1}^{q_k} \alpha_i^k \exp(\beta_i^k \tau / \Delta t). \quad (16)$$

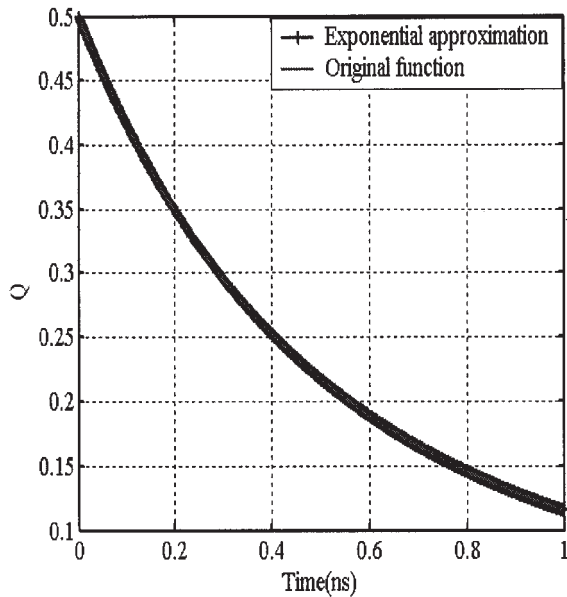


Figure 4 Exponential approximation for Q . Conductivity = 0.1 s/m, $q = 4$, $R = 0$

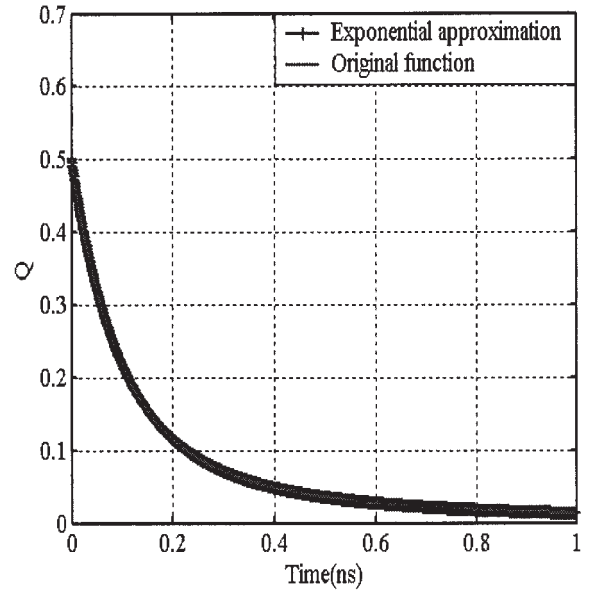


Figure 5 Exponential approximation for Q . Conductivity = 0.5 s/m, $q = 4$, $R = 0$

This form enables a recursive formulation of the convolution

$$\int_0^{t-R/c} Q(\tau, R) * F(t - \tau - R/c) d\tau = A \sum_{i=1}^q \Psi^{i,t} = A \sum_{i=1}^q [\alpha_i (\exp(\gamma_i) - 1) F(t_i) + \exp(\gamma_i) \psi^{i,t-1}], \quad \gamma_i = B\beta_i. \quad (17)$$

Consequently, at each time step, instead of computing the temporal convolution directly, only a single summation independent of number of time steps is needed to update the convolution. This

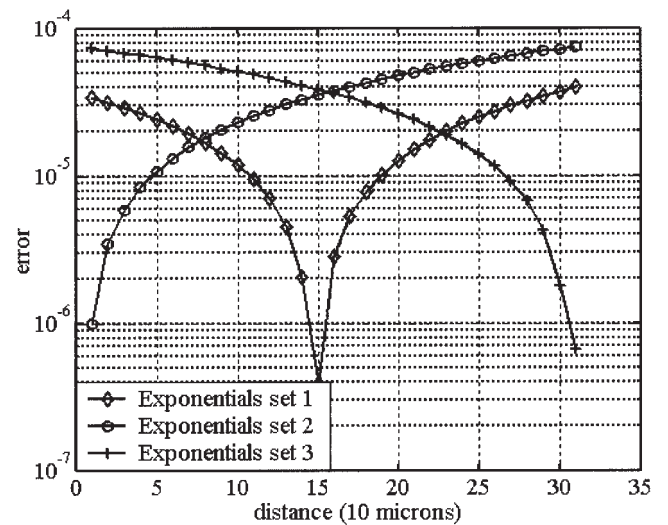


Figure 6 Relative error between exponential approximations and original function. Exponentials set 1 was derived by setting $R = 150$ microns; exponentials set 2 was derived by setting $R = 0$ microns; exponentials set 3 was derived by setting $R = 300$ microns

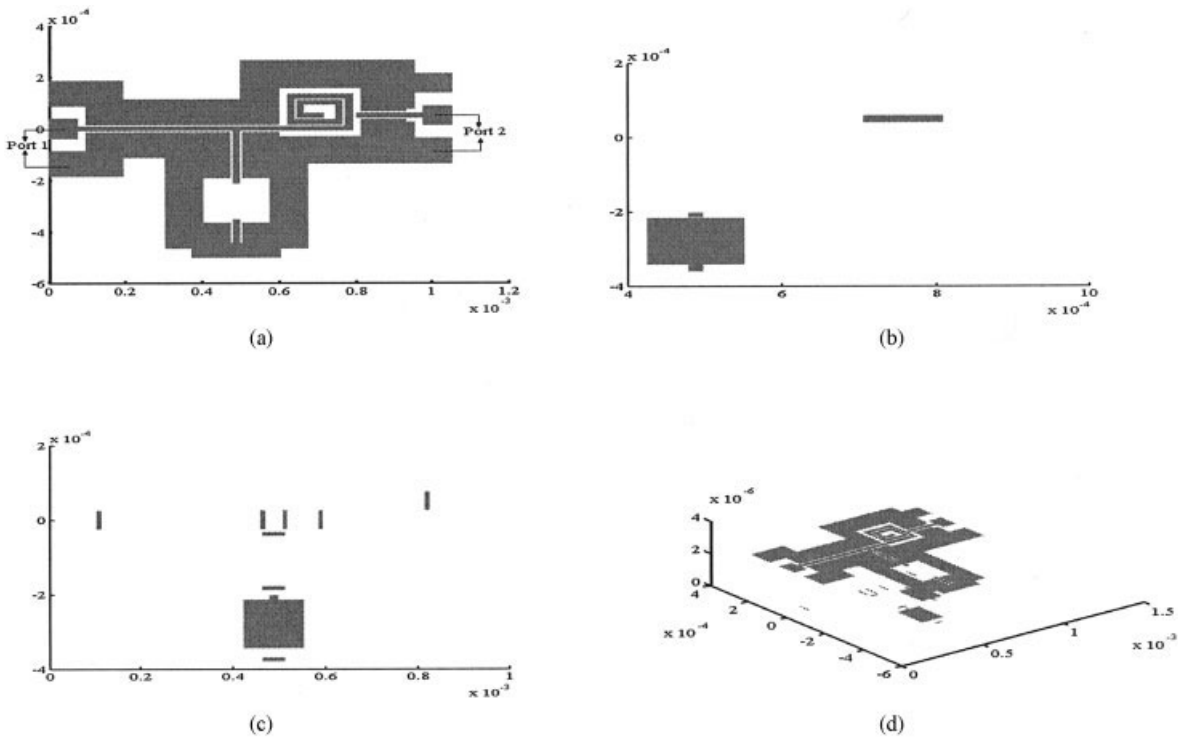


Figure 7 LC matching network: (a) first layer; (b) second layer; (c) third layer; (d) 3D view

then achieves the purpose of reducing computational complexity to be similar to that of a TDIE solver for lossless media.

As shown in Figures 4 and 5, the exponential approximations show excellent match to the original $Q(\tau, R)$ function. As discussed previously, for realistic substrate sizes and losses, only a small number of sets of fitting exponentials are needed to accurately represent $Q(\tau, R)$. In fact, as Figure 7 shows, for substrates with linear dimensions of $300 \mu\text{m}$, only one set of exponentials might be sufficiently accurate to represent $Q(\tau, R)$.

3. NUMERICAL RESULTS

In the simulation example, the effect of lossy substrate on the performance of a X-band low-noise amplifier was simulated. The time-domain coupled solver was used to extract scattering parameters of a two-port system. Two simulation cases were run using the time-domain solver. One case is without the substrate, while

the other is with the lossy substrate. Then the simulation result from the time-domain coupled solver was compared with the measurement data and those from its frequency-domain counterpart [27, 28]. The two-port system under study is an LC matching network for an X-band low noise amplifier. As shown in Figures 7 and 8, the network contains an MIM capacitor, a planar spiral inductor, a coplanar waveguide tee, a coplanar waveguide, and input/output transmission lines. The physical parameters for the layer stack are shown in Table 1.

Based upon the fact that the skin depth of the metal layers are much larger than the thickness of the layers, all the metal layers are treated as infinitely thin 2D structures. Figure 9 indicates that the simulation result is closer to the measured data when the effect of the lossy substrate is included in the modeling.

ACKNOWLEDGMENTS

This work was partially supported by DARPA-MTO NeoCAD grant no. N66001-01-1-8920, NSF-CAREER grant no. ECS-0093102, and NSF-SRC Mixed-Signal Initiative grant no. CCR-0120371. The authors would like to thank Swagato Chakraborty for providing the frequency-domain simulation results.

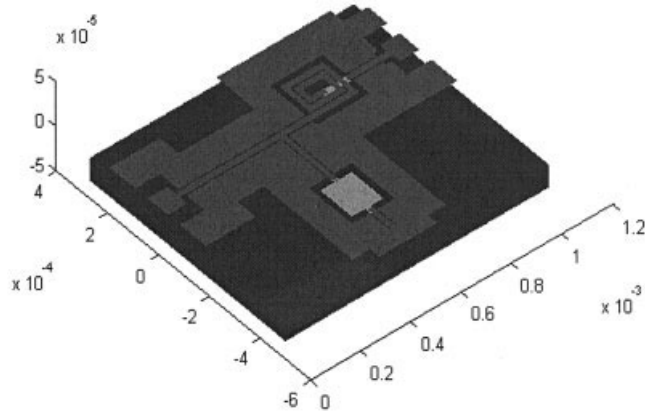


Figure 8 Three-dimensional view of LC matching network with lossy substrate

TABLE 1 Physical Parameters for the Layer Stack

	ϵ_r	Thickness	σ
Air	1.0	—	—
Metal-layer 1	—	$0.2 \mu\text{m}$	$3.33e + 7 \text{ S/m}$
Oxide	4.0	$1.5 \mu\text{m}$	—
Metal-layer 2	—	$0.6 \mu\text{m}$	$1.32e + 7 \text{ S/m}$
Oxide	4.0	$1.0 \mu\text{m}$	—
Metal-layer 3	—	$0.6 \mu\text{m}$	$1.32e + 7 \text{ S/m}$
Oxide	4.0	$0.845 \mu\text{m}$	—
Lossy substrate	11.9	$675 \mu\text{m}$	5.0 S/m

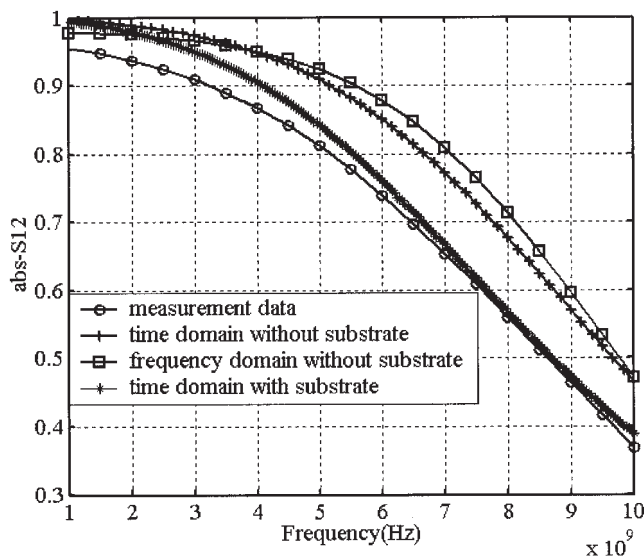


Figure 9 The $\text{abs-}S_{12}$ of an LC matching network

REFERENCES

1. I. Erdin, M.S. Nakhla, and R. Achar, Circuit analysis of electromagnetic radiation and field coupling effects for networks with embedded full-wave modules, *IEEE Trans Electromagn Compat* 42 (2000), 449–460.
2. C. Kuo, B. Houshmand, and T. Itoh, Full-wave analysis of packaged microwave circuits with active and nonlinear devices: An FDTD approach, *IEEE Trans Microwave Theory Tech* 45 (1997), 819–826.
3. B. Toland, J. Lin, B. Houshmand, and T. Itoh, FDTD analysis of an active antenna, *IEEE Trans Microwave Guided Lett* 3 (1993), 423–425.
4. S. Chang, R. Coccioli, Y. Qian, and T. Itoh, A global finite-element time-domain analysis of active nonlinear microwave circuits, *IEEE Trans Microwave Theory Tech* 47 (1999), 2410–2416.
5. K. Guillouard, M.F. Wong, V.F. Hanna, and J. Citerne, A new global time-domain electromagnetic simulator of microwave circuits including lumped elements based on finite-element method, *IEEE Trans Microwave Theory Tech* 47 (1999), 2045–2048.
6. H. Heeb and A.E. Ruehli, Three-dimensional interconnect analysis using partial element equivalent circuits, *IEEE Trans Circ Syst I Funda Theory Applic* 39 (1992), 974–982.
7. W. Pinello, A.C. Cangellaris, and A. Ruehli, Hybrid electromagnetic modeling of noise interactions in packaged electronics based on the partial-element equivalent-circuit formulation, *IEEE Trans Microwave Theory Tech* 45 (1997), 1889–1896.
8. P.J. Restle, A.E. Ruehli, S.G. Walker, and G. Papadopoulos, Full-wave PEEC time-domain method for the modeling of on-chip interconnects, *IEEE Trans CAD Integrated Circ Syst* 20 (2001), 877–866.
9. A.E. Ruehli, G. Antonini, J. Esch, J. Ekman, A. Mayo, and A. Orlandi, Nonorthogonal PEEC formulation for time- and frequency-domain EM and circuit modeling, *IEEE Trans Electromagn Compat* 45 (2003), 167–176.
10. C. Yang and V. Jandhyala, A time-domain surface integral technique for mixed electromagnetic and circuit simulation, *Proc IEEE Electrical Perf Electron Packaging*, Monterey, CA, 2002, pp. 41–44.
11. C. Yang and V. Jandhyala, Coupled circuit-electromagnetic simulation with time-domain integral equations, *Proc IEEE APS Dig 3 Columbus, OH*, 2003, pp. 316–319.
12. C. Yang and V. Jandhyala, Integral equation based time domain coupled EM-circuit simulation for packaged conductors and dielectrics, *Proc IEEE Electrical Perf Electron Packaging*, Princeton, NJ, 2003, pp. 371–374.
13. K. Aygun, B. Shanker, A.A. Ergin, and E. Michielssen, A fast time domain integral equation technique for analyzing EMC/EMI problems,

IEEE International Symposium, Antennas and Propagation Society 2 (1999), 1366–1369.

14. K. Aygun, B.C. Fisher, J. Meng, and E. Michielssen, A fast hybrid field-circuit simulator for transient analysis of microwave circuits, *IEEE Trans Microwave Theory Tech* 52 (2004), 573–583.
15. M.J. Bluck, S.P. Walker, and M.D. Pockock, The extension of time-domain integral equation analysis to scattering from imperfectly conducting bodies, *IEEE Trans Antennas and Propagation*, 49 (2001), 875–879.
16. A.E. Yilmaz, D.S. Weile, B. Shanker, J.-M. Jin, and E. Michielssen, Fast analysis of transient scattering in lossy media, *Antennas Wireless Propagat Lett* 1 (2002), 14–17.
17. E. Schlemmer, W.M. Rucker, and K.R. Richter, Boundary element computations of 3-D transient scattering from lossy dielectric objects, *IEEE Trans Magn* 29 (1993), 1542–1547.
18. P. Jiang and E. Michielssen, Temporal acceleration of time-domain integral-equation solvers for electromagnetic scattering from objects residing in lossy media, *Microwave Opt Techn Lett* 10 (2005), 223–230.
19. S.M. Rao and T.K. Sarkar, Numerical solution of time domain integral equations for arbitrarily shaped conductor/dielectric composite bodies, *IEEE Trans Antennas Propagat* 50 (2002), 1831–1837.
20. P.M. Morse and H. Feshbach, *Methods of theoretical physics*, McGraw-Hill, New York, 1953.
21. G. Manara, A. Monorchio, and R. Reggiannini, A space-time discretization criterion for a stable time-marching solution of the electric field integral equation, *IEEE Trans Antennas Propagat* 45 (1997), 527–532.
22. D.S. Weile, G. Pisharody, N.W. Chen, B. Shanker, and E. Michielssen, A novel scheme for the solution of the time-domain integral equations of electromagnetics, *IEEE Trans Antennas Propagat* 52, 283–295.
23. J.G. Maloney and G.S. Smith, The use of surface impedance concepts in the finite-difference time-domain method, *IEEE Trans Antennas Propagat* 40 (1992), 38–48.
24. K.S. Oh and J.E. Schutt-Aine, An efficient implementation of surface impedance boundary conditions for the finite-difference time-domain method, *IEEE Trans Antennas Propagat* 43 (1995), 660–666.
25. C.R. Paul, *Analysis of multiconductor transmission lines*, Wiley, c1994.
26. K.S. Kunz and R.J. Luebbers, *The finite difference time domain method in electromagnetics*, CRC Press, Boca Raton, FL, 1993.
27. Y. Wang, D. Gope, V. Jandhyala, and C.J. Richard Shi, Generalized Kirchoff's current and voltage law formulation for coupled circuit-electromagnetic simulation with surface integral equations, *IEEE Trans Microwave Theory Tech* 52 (2004), 1673–1682.
28. Y. Wang, V. Jandhyala, and C.J. Richard Shi, Coupled electromagnetic-circuit simulation of arbitrarily shaped conducting structures, *Proc IEEE Electrical Perf Electron Packaging*, Boston, MA, 2001, pp. 233–236.

© 2005 Wiley Periodicals, Inc.

BROADBAND 40-GHz COHERENT SOURCE BASED ON SUPERCONTINUUM GENERATION IN HIGHLY NONLINEAR FIBER

Ge Xia, Dexiu Huang, Xiaogang Chen, and Xiuhua Yuan

Department of Optoelectronics Engineering
Huazhong University of Science and Technology
Wuhan, 430074, P. R. China

Received 26 March 2005

ABSTRACT: A broadband 40-GHz coherent source, which utilizes supercontinuum (SC) generated in highly nonlinear fiber (HNLF) with large normal dispersion is investigated for the first time. In order to enhance the SC generation in the HNLF, a new scheme that applies the